

Study of the mechanism of the beam-beam limit

K. Ohmi, M. Tawada and K. Oide
KEK, Oho, Tsukuba, 305-0801, Japan

The beam-beam limit is a key issue both in operation and design of e^+e^- factories. The luminosity is limited by saturation of the beam-beam parameter. Two type of possibilities, in which coherent and/or incoherent effects causes the limit, are discussed. One is the coherent motion between the two beams, in which the betatron oscillations of the two beams coupled and a mode becomes unstable. The other is incoherent beam size enlargement due to the nonlinear force of the beam-beam interactions. The coherent motion is linear effect in the lowest approximation, and the nonlinear force, if anything, make suppress the coherent motion. The incoherent effect is essentially nonlinear. The beam-beam force has a large tune shift which means a strong linear coupling of the two beam, while it has also a strong nonlinearity: i.e., the tune spread is the same order as the tune shift. Therefore it is very interesting how these two effects behave in the beam-beam phenomenon. We discuss the beam-beam limit from the viewpoint both of the coherent and incoherent effects using computer simulations.

1. Introduction

The beam-beam limit is characterized by so-called the beam-beam parameter, which is defined by

$$\xi_{x(y),\pm} = \frac{N_{\mp} r_e}{\gamma_{\pm}} \frac{\beta}{\sigma_{x(y)}(\sigma_x + \sigma_y)}. \quad (1)$$

It increases proportional to the beam current for low beam current at which the beam sizes are kept. However the beam-beam parameter increases with a slower rate or is saturate at a value, once the bunch current exceeds a threshold. This phenomenon is called the beam-beam limit. Actually the beam-size is enlarged by the beam-beam interaction over the threshold, with the result that the beam-beam parameter and the luminosity is reduced to be less than the geometrical value. The luminosity is expressed by

$$L = \frac{N_+ N_- f}{4\pi\sigma_x\sigma_y} \approx \frac{\gamma_{\pm}}{2r_e} \left(\frac{N_{\pm}\xi_{y,\pm}}{\beta_{y,\pm}} \right) f_{rep}. \quad (2)$$

We try to understand and predict the beam-beam limit using computer simulations. There is no analytic method to predict the limit value with a sufficient accuracy, because it is a strong nonlinear phenomenon. Two types of simulation methods are used to study. One is weak-strong simulation in which one beam is assumed to be fixed charge distribution and another beam is represented by macro-particles. Second is strong-strong simulation in which both beams are represented by macro-particles. Weak strong simulations had been used to design particle factories, because strong-strong simulations have been suffered by numerical noise due to poor computer power in those days. It is not clear whether the weak-strong simulation can predict the beam-beam limit. Above all, we do not understand the mechanism of the beam-beam limit, therefore we did not know which method predict the beam-beam limit. The strong-strong simulation can take into account all of possible mechanism by which the beam-beam limit is caused.

The beam-beam limit is considered to be caused by coherent motion or incoherent effects. Which effect is essential depends on the parameters. We discuss how the effect play roles in the beam-beam limit. Parameter used in our study is shown in Table I.

| | | LER | HER | |
|---------------------------|--------------|------------------------|------|-------------------------------|
| Beam Energy | E | 3.5 | 8.0 | GeV |
| Beam current | I | 9.4 | 4.1 | A |
| Particles/bunch | N | 11.8 | 5.13 | $\times 10^{10}$ |
| Number of bunches | N_b | 5018 | | |
| Horizontal emittance | ϵ_x | 18 - 33 | | nm |
| Vertical emittance | ϵ_y | 0.18 - 0.33 | | nm |
| Bunch length | σ_z | 3 | | mm |
| Horizontal β at I.P | β_x | 15 - 30 | | cm |
| Vertical β at I.P | β_y | 3 | | mm |
| Crossing angle | θ_x | 0(crab cav.) - 30 | | mrads |
| Beam-beam parameter | ξ | 0.05 - 0.26 | | |
| Circumference | C | 3016.26 | | m |
| Luminosity | L | $1 - 6 \times 10^{35}$ | | $\text{cm}^{-2}\text{s}^{-1}$ |

Table I Machine parameters of SuperKEKB.

2. Beam-beam limit due to coherent motion

The coherent motion discussed here is a collective betatron motion with a correlation of two beams. Spectra of the coherent modes are discussed in Refs.[1, 2]. Tune difference between π - σ mode spectra were main subject. The beam-beam limit due to the coherent π mode was discussed in Ref. [3] for KEKB. The study is performed by a strong-strong simulation in two-dimensional space.

In our parameter, coherent instability is observed for only case of short bunch length or in two dimen-

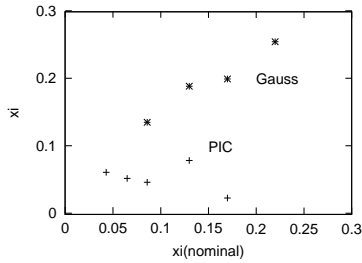


Figure 1: Beam-beam parameter estimated by luminosity for various current. Cross and diamond points denote the beam-beam parameter given by PIC and Gaussian models, respectively.

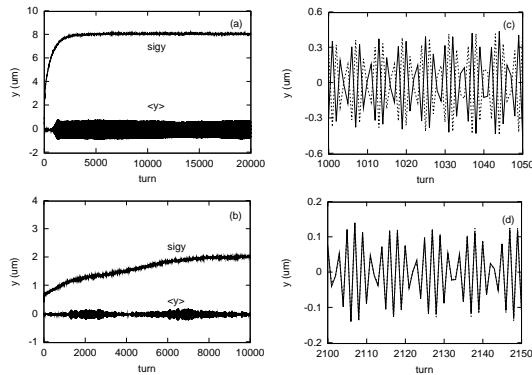


Figure 2: Evolution of vertical beam size and dipole amplitude. The beam size and dipole amplitude given by PIC and Gaussian models are depicted in pictures (a) and (b), respectively. Dipole motions during shorter period, which are depicted in the picture (c) and (d), shows coherent mode.

sional simulation. Figure 1 shows the beam-beam parameter obtained by two-dimensional Gauss and PIC models. Gauss model shows unlimited beam-beam parameter at least up to 0.2, while PIC method gives a beam-beam limit around 0.05. Figure 2 shows the vertical beam size and dipole amplitude given by PIC and Gaussian models. In PIC model, the dipole amplitude grows about design beam size $\sim 1 \mu\text{m}$ and the rms vertical beam size also grows as is shown in picture (a). The coherent instability, which is observed for larger beam-beam parameter than 0.05, causes the beam-beam limit. Such a coherent instability has been seen in several strong-strong code with PIC model [4]. Gaussian model does not show remarkable coherent motion as is shown in picture (b). Pictures (c) and (d) show detail structures of the dipole motion for PIC and Gaussian models. PIC model gives motion of the coherent π mode, while Gauss model gives σ mode. These features reflect the behavior of the beam-beam limit in Figure 1.

Figure 3 shows Fourier amplitude of the dipole moment in the Gaussian and PIC models. σ and π mode spectra are seen in the both models, but their behav-

iors are different. σ mode always enhances for π mode but does not grow remarkably in the Gaussian model, therefore the beam-beam system is kept to be stable. In the PIC model, π mode enhances for σ mode and grows strongly for high current.

Though the behavior may depend on tune operating point, such remarkable difference is interesting and may be a suspicious feature of the Gaussian model.

The coherent motion are expected to be smeared for an operation with different tune. Figure 5 shows luminosity evolution for an operation with different tune. The tune operating points are (0.506,0.545) and (0.515,0.58) for LER and HER, respectively. These operating points are used at the present KEKB. The figure shows that the luminosity is recovered by the tune difference.

There were many discussions whether the PIC model is reliable for stability during several thousand turn. Numerical noise may enhance coherent motions or particle diffusion. The feature of the coherent motion is confirmed by several codes [4] as is already mentioned, and is not changed for statistics and choice of mesh in PIC model. A numerical diffusion is examined using weak-strong simulations [5]. Luminosity and vertical beam size obtained by simulations with the exact formula [6] and PIC method are compared for a given Gaussian strong beam. Figure 6 shows the luminosity and beam size evolutions for exact formula and for PIC method. There is no problem for the numerical diffusion of PIC model.

We take into account the bunch length in the beam-beam effect. Three dimensional simulation is performed to take into account. Crossing angle is not considered first. Figure 7 shows luminosity evolution for some cases of bunch lengths. Two levels of beam-beam parameter are seen in the figure: one is 0.1 for $\sigma_z = 1.5 \text{ mm}$ and another is 0.03 for $\sigma_z = 0.3, 0.6$ and 1 mm . The beam-beam parameter for the short bunch length $\sigma_z \leq 1 \text{ mm}$ is similar as that obtained by the two-dimensional simulation. The coherent motion seen in the two-dimensional simulation is observed for the cases of short bunch length. The beam-beam parameter for $\sigma_z = 1.5 \text{ mm}$ is also similar as that of the design value, $\sigma_z = 3 \text{ mm}$. The coherent motion disappears for longer bunch length $\geq 1.5 \text{ mm}$. The threshold of the bunch length seems to be about $\beta_y/2$, since the vertical beta function is 3 mm . This result may be due to spread of beam-beam tune shift along the longitudinal direction.

3. Incoherent effect

As is shown in previous section, coherent motion disappear due to some reason: smear due to nonlinearity or frequency spread seems to be one of the major reason. In this case, what kind of mechanism can

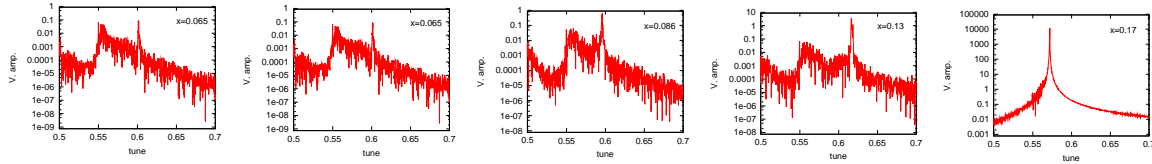


Figure 3: Fourier spectra for the vertical dipole motion obtained by PIC model. Pictures (a)-(e) are depicted for the nominal beam-beam parameter, $\xi = 0.043, 0.065, 0.086, 0.13$ and 0.17 .

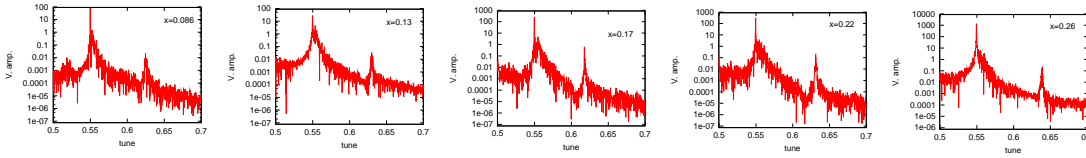


Figure 4: Fourier spectra for the vertical dipole motion obtained by Gauss model. Pictures (a)-(e) are depicted for the nominal beam-beam parameter, $\xi = 0.086, 0.13, 0.17, 0.22$ and 0.26 .

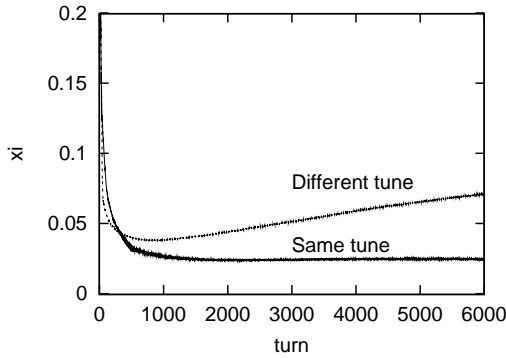


Figure 5: Evolution of the beam-beam parameter for different tune. LER and HER are operated with the tune, $(0.506, 0.545)$ and $(0.515, 0.58)$, respectively.

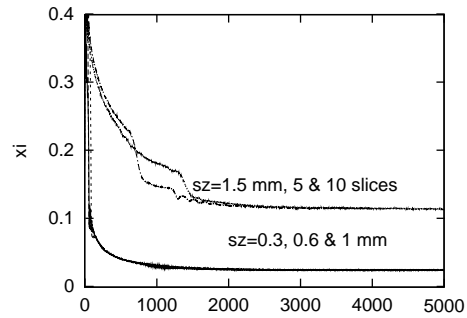


Figure 7: Evolution of luminosity for various bunch length. For $\sigma_z = 1.5$ mm, the simulations are performed for numbers of slices, 5 and 10 with the PIC method.

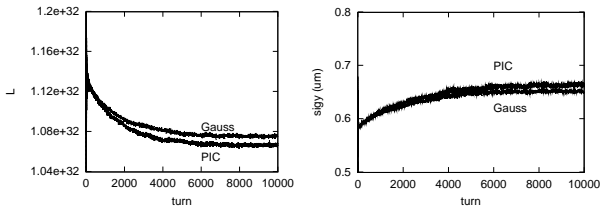


Figure 6: Evolution of luminosity and vertical beam size given by weak-strong simulation using PIC method and exact solution for a Gaussian strong beam distribution.

limits the luminosity? Actually, the beam-beam parameter for long bunch shown in Figure 7 is limited around 0.1. Any coherent motion was not observed in the simulations: some kind of incoherent effects limit the beam-beam parameter. We discuss beam-beam limit due to the incoherent effects.

Figure 8 shows the beam-beam parameter and beam sizes for various current obtained by Gaussian and PIC model. The horizontal axis in the figure is represented by so-called nominal beam-beam parameter

calculated by Eq.(1). The results given by the Gaussian approximation and by the PIC method are very different. Remarkable enlargement was not seen in the horizontal beam size, but was seen in the vertical beam size. The enlargement given by the PIC method was stronger than that by the Gaussian approximation. Gaussian approximation gave a high beam-beam parameter of more than 0.2, while the PIC method gave saturation of the beam-beam parameter around 0.1. No coherent motion was seen in first and second moments: $\langle x_i \rangle$ and $\langle x_i x_j \rangle$ in both methods. The weak-strong simulation with Gaussian fixed beam [7] gave similar results as the Gaussian strong-strong simulation. Figure 9 shows the evolution of the luminosity for various current obtained by the PIC simulation. The behavior of luminosity is gentle for $\xi = 0.04$ and 0.08 , while sudden changes are sometimes seen for $\xi \geq 0.12$.

Figure 10 shows the variation of the particle distribution during the sudden change of the luminosity. Both of electron and positron distributions are depicted in the figure. Both distributions are enlarged and distorted from a Gaussian simultaneously while

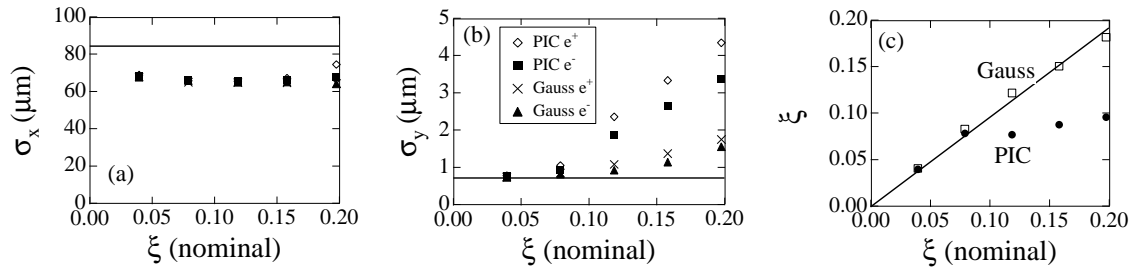


Figure 8: Beam sizes and the beam-beam parameter function of the nominal beam-beam parameter obtained by the strong-strong simulations with the particle-in-cell method and Gaussian approximation. Horizontal and vertical beam sizes are depicted in (a) and (b). Effective beam-beam parameters are depicted in (c).

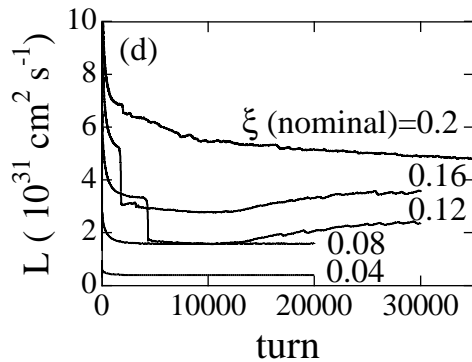


Figure 9: Evolution of luminosity for various current.

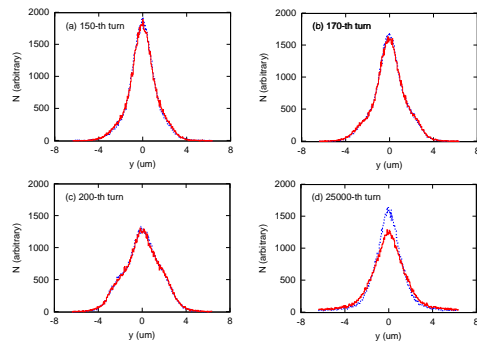


Figure 10: Evolution of the vertical distribution of electron and positron beams. The distributions after 150, 170, 200 and 30,000 turns are depicted in picture (a), (b), (c) and (d), respectively.

overlapping each other. The final distributions after 25,000 turns are seen in Figure 10(d). The distribution of positrons is slightly broader than that of electrons, due to the difference in the radiation damping time. Both distributions, which are distorted from a Gaussian mainly in the tail part, are considered as an equilibrium distribution of the two colliding beams.

We now think that the beam-beam limit is determined by the equilibrium distribution of two beams, but is not caused by coherent motion. To confirm

this idea, we executed a weak-strong simulation using the particle distribution obtained by the strong-strong simulation. If the beam size enlargement is due to an incoherent phenomenon, the same results of luminosity and size should be obtained in the final stage. The strong beam, which is the electron beam in the figure, is given by the final distribution of the strong-strong simulation using the PIC code, while the weak positron beam is initialized with the designed Gaussian distribution. In this approach, any coherent motion, even a small breathing, is suppressed. Figure 11 shows the evolution of luminosity and beam size given by the weak-strong simulation. The luminosity is at a similar level after 40,000 turns as that of the strong-strong simulation as is shown in Figure 11(a). The evolution of the beam sizes for the weak-strong and strong-strong simulations are shown in Figure 11(b) and (c), respectively. The size of the positron beam in the two simulations grows to the closed value. The two luminosities do not coincide perfectly, but have a difference of 15%. Figure 11 (d) shows the evolution of the size of the positron beam that interacts with a fixed Gaussian electron beam. The beam size is much less than that for the distorted beam. This means that the distortions are destructive to each other: if one beam is distorted from a Gaussian, the other beam is forcefully distorted as well.

It is interesting to see Poincaré plot for the distorted and Gaussian distribution in the weak-strong simulation. Figure 12 shows that Poincaré plot in $y - p_y$ phase space. This and next two figures are obtained by two-dimensional simulation for the simplicity. Ten particles without x and z amplitudes are tracked with interacting the three types of beam: distorted distribution obtained by the strong-strong simulation, Gaussian distribution whose force are calculated by PIC method, and Gaussian whose force is calculated by exact formula with complex error function, where the radiation damping and excitation are cut. The results of pictures (b) and (c) given by PIC and exact formula, respectively for Gaussian distribution well coincide. The trajectories in picture (a) for distribution obtained by the strong-strong simulation

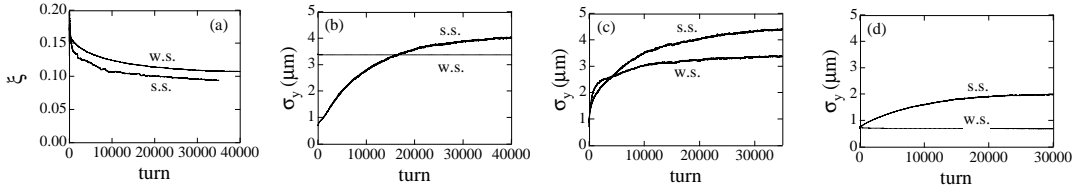


Figure 11: Evolution of the beam-beam parameter and vertical size of electron (blue) and positron (red) beams. Evolutions of ξ for the weak-strong and strong-strong simulation is depicted in (a), where the final distribution of the strong-strong simulation is used as fixed distribution in the weak-strong simulation. Evolutions of the beam size for weak-strong and strong-strong simulations are depicted in (b) and (c), respectively. Evolution of the size of positron beam that interacts with fixed Gaussian electron beam is depicted in (d).

is different from pictures (b) and (c) for Gaussian, but They do not give clear information for the mechanism of the beam-beam limit.

We next discuss the diffusion of the beam-beam system. Figures 13 and 14 show evolution for the beam-beam parameter and vertical beam size, respectively. In each pictures, the evolutions in the case of including the damping and excitation of synchrotron radiation and of Hamiltonian system without the radiation are depicted. Three pictures in each figure are depicted for distorted distribution obtained by the strong-strong simulation, Gaussian distribution whose force are calculated by PIC method, and Gaussian whose force is calculated by exact formula with complex error function. For the beam-beam system without synchrotron radiation, luminosity and beam size are kept to be an initial value: namely, diffusion due to nonlinearity is weak. The behaviors in the case of including the radiation are different each other. They have already been seen in Figure 11. Synchrotron radiation play an important role for the beam-beam limit. Additionally, structure of the phase space for the distorted distribution is sensitive for the diffusion.

4. Crossing angle

In present KEKB, finite crossing angle scheme has been adopted. Achievement of the design luminosity $10^{34} \text{ cm}^{-2}\text{s}^{-1}$ at KEKB showed that the finite crossing angle scheme was no problem to achieve the beam-beam parameter up to 0.05. In previous section, the beam-beam limit without crossing angle was about 0.1 in the three dimensional simulation. The crossing collision scheme should be reviewed in the point of view of progress toward higher luminosity. Crab cavity makes collision with finite crossing angle possible to pretend to be that of zero crossing angle. This study gives an answer whether the crab cavity should be installed.

The collision with crossing angle is treated by Lorenz boost to a head-on frame from the laboratory frame [8, 9]: i.e., particles in the beam are transferred

to the head on frame, experience the collision, and are transferred to laboratory frame by the inverse of the Lorenz boost. In the laboratory frame, s axes of two beams are chosen to be their moving directions, and the electro-magnetic field of a beam is formed on the plane perpendicular to its s axis. The beam-beam force which the other beam experiences is not transverse direction, and the timing when the beam experiences the force depends on the positions of the two beams. In the head-on frame, s axes of two beams are coincide except that their directions are opposite. Beam particles in the two beams basically move along s direction and beam-beam force is perpendicular to s axis. The principle axis of the beam ellipsoid does not coincide with s direction: that is, $\langle xz \rangle$ is not zero for the case of horizontal crossing.

The Lorenz transformation from the laboratory frame to the head-on frame is given for a half crossing angle θ by

$$\begin{aligned}
 x^* &= \tan \theta z + \left(1 + \frac{p_x^*}{p_s^*} \sin \theta\right) x \\
 y^* &= y + \sin \theta \frac{p_y^*}{p_s^*} x \\
 z^* &= \frac{z}{\cos \theta} - \frac{H^*}{p_s^*} \sin \theta x \\
 p_x^* &= \frac{p_x - \tan \theta H}{\cos \theta} \\
 p_y^* &= \frac{p_y}{\cos \theta} \\
 p_z^* &= p_z - \tan \theta p_x + \tan^2 \theta H,
 \end{aligned} \tag{3}$$

where

$$\begin{aligned}
 H &= (1 + p_z) - \sqrt{(1 + p_z)^2 - p_x^2 - p_y^2} \\
 p_s &= \sqrt{(1 + p_z)^2 - p_x^2 - p_y^2}
 \end{aligned}$$

. A star designates a dynamical variable in the head-on frame. H^* and p_s^* are $H(\mathbf{p}^*)$ and $p_s(\mathbf{p}^*)$, respectively. Note that the x^* and y^* axes are defined in the same direction for both beams, while the s^* axis

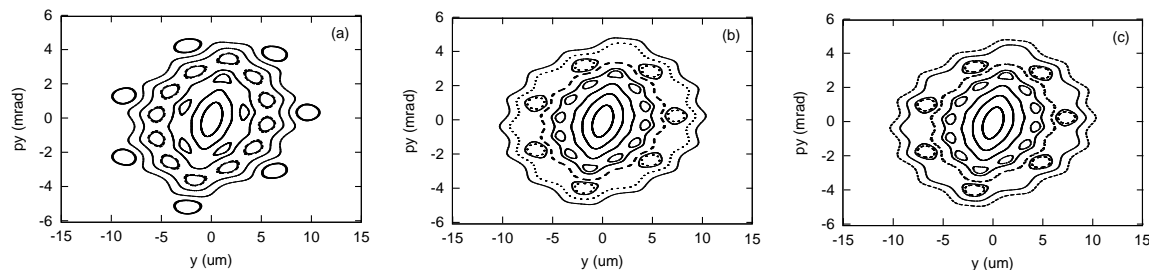


Figure 12: Poincaré plot for the distorted and Gaussian distributions given by two-dimensional simulation. Picture (a) is obtained by PIC method for the distorted distribution. Pictures (b) and (c) are obtained by PIC method and exact error function formula, respectively, for Gaussian distribution.

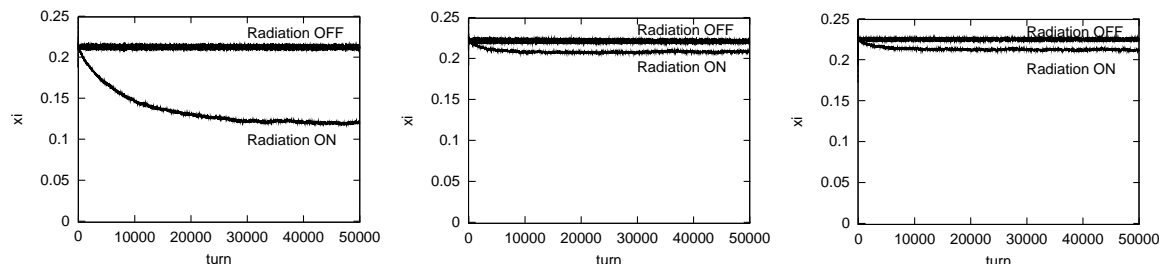


Figure 13: Evolution of the beam-beam parameter given by the two dimensional simulation. Two lines which correspond to ON/OFF of the synchrotron radiation are depicted. Picture (a) is obtained by PIC method for the distorted distribution. Pictures (b) and (c) are obtained by PIC method and exact error function formula, respectively, for Gaussian distribution.

is defined in opposite directions, since the two beams travel in opposite directions.

The linear part of the transformation is expressed by a matrix

$$M_{crs} = \begin{pmatrix} 1 & 0 & 0 & 0 & \tan \theta & 0 \\ 0 & 1/\cos \theta & 0 & 0 & 0 & 0 \\ 0 & 0 & 1 & 0 & 0 & 0 \\ 0 & 0 & 0 & 1/\cos \theta & 0 & 0 \\ 0 & 0 & 0 & 0 & 1/\cos \theta & 0 \\ 0 & -\tan \theta & 0 & 0 & 0 & 1 \end{pmatrix}. \quad (4)$$

These transformations are not symplectic: determinant of the transfer matrix M_{crs} is not 1, but $\cos^{-3} \theta$. The fact is due to that Lorentz transformation is not symplectic for the accelerator coordinate, because the Hamiltonian is divided by a reference momentum. This is not problem because the inverse factor of $\cos^3 \theta$ is applied by the inverse transformation.

By including this transformation Eq.(3) or (4) into the map of arc section, the simulation is done without any change, except that the beam shape has gradient in the $x - z$ plane. The gradient is considered automatically in the three dimensional simulation.

Figure 15 shows the relation of the beam-beam parameter ξ and the bunch population for collision with and without crossing angle, where a half crossing angle is 11 mrad. These simulations are performed with present KEKB parameter: that is, β_x/β_y is 60/0.7 cm

and $\sigma_z = 0.7$ cm. Pictures (a) and (b) were obtained by the weak-strong and strong-strong simulations, respectively. The beam-beam limit is 0.1 or > 0.2 for collision without crossing angle as is discussed in the previous section. ξ at crossing collision is similar behavior for the both of two simulations: that is, ξ is saturated around 0.06.

Figure 16 shows the beam-beam parameter for various crossing angle. The geometrical luminosity, which is also plotted in the figure, has loose dependence for the crossing angle. The simulated luminosity is peak structure near zero-crossing angle for the simulations. The peak structure of the strong-strong simulation is narrower than that of the weak-strong simulation.

The beam-beam parameters at 11 mrad for the weak-strong and strong-strong simulations coincided each other, while they do not coincide for other crossing angles. Probably the coincidence is accidental.

These results suggest that the collision performance for zero crossing angle is much better than that of finite crossing angle. Crab cavity creates a kind of dispersion $x = \zeta_x z$ concerning z . The dispersion corresponds to (1,5) and (6,2) components of the transfer matrix, which has the same structure as that between the laboratory and head-on frames for collision of finite crossing angle. This means that the collision with a finite crossing angle can be replaced by that with zero crossing angle using crab cavities effectively. These results show that crab cavities improve

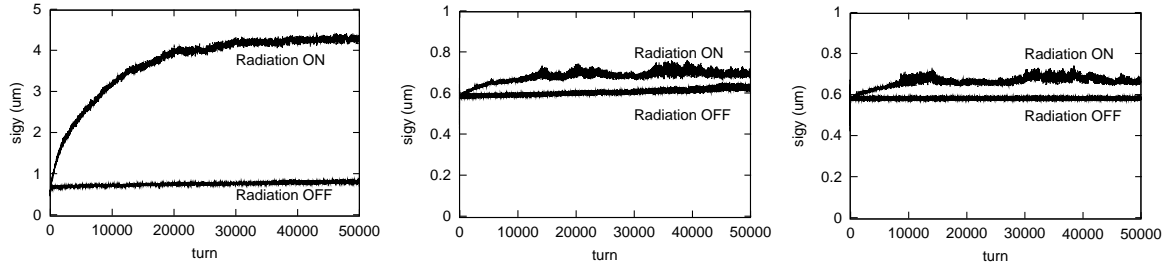


Figure 14: Evolution of the vertical beam size given by the two dimensional simulation. Two lines which correspond to ON/OFF of the synchrotron radiation are plotted. Picture (a) is obtained by PIC method for the distorted distribution. Pictures (b) and (c) are obtained by PIC method and exact error function formula, respectively, for Gaussian distribution.

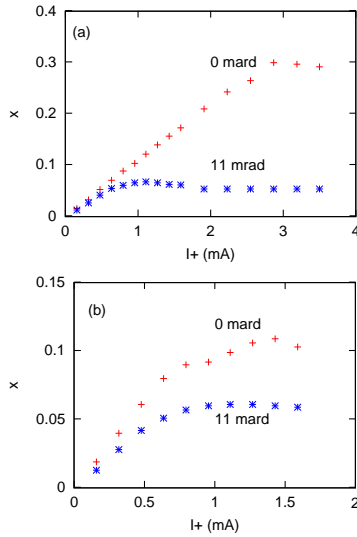


Figure 15: Beam-beam parameters for zero and finite crossing angle. Picture (a) and (b) are obtained by the weak-strong and strong-strong simulations, respectively.

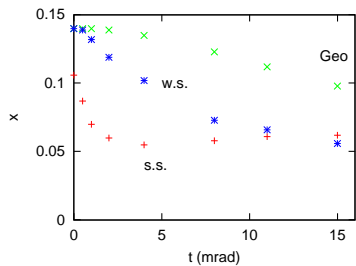


Figure 16: Beam-beam parameters for various crossing angle. Three points depict geometrical luminosity and those given by the weak-strong and strong-strong simulations.

the luminosity drastically.

The reason why the crossing angle makes worse the luminosity is discussed now. We focus the nonlinear diffusion as is done in previous section. The weak-strong simulation with Gaussian model is used here.

Needless to say, it is better to use the distribution obtained by the strong-strong simulation. The PIC weak-strong code is under-construction. Figure 17 shows evolution of the luminosity for zero and finite crossing angles. Pictures (a) and (b) are depicted luminosity evolutions with/without synchrotron radiation damping, respectively, for tune operating point of (0.508,0.55). The operating point is closed to that of LER for the present KEKB. For zero crossing angle, diffusion due to nonlinearity is not seen as is discussed in previous section. For finite crossing angle, diffusion is clearly seen. Including the synchrotron radiation, the diffusion is emphasized further more. Pictures (c) and (d) are depicted for the tune operating point (0.518,0.58). The operating point is closed to that of HER for the present KEKB. The diffusion rate due to nonlinearity, which depends on the operating point, is worse than previous operating point. The beam-beam limit or total diffusion including synchrotron radiation is also worse than the previous point.

The crossing angle makes an occurrence of the nonlinear diffusion in both of vertical and horizontal beam sizes. Figure 18 shows the diffusion of the horizontal and vertical beam sizes due to the crossing angle. It is interesting that the crossing angle which causes linear $x-z$ coupling also affects the vertical diffusion. A slight diffusion is seen for zero crossing angle. It is not seen at all in two-dimensional simulation as shown in Figure 18 (c).

Similar diffusion is also caused by $x-y$ coupling. Figure 19 shows that diffusion seen in the beam-beam parameter with $x-y$ coupling, $r_4 = 0.4$. Nonlinear diffusion seen in picture (a) shows an interesting feature. The strength of the diffusion is different between two and three dimensional simulation: i.e. it is weak for 2 dim. but is clear for 3 dim. Number of dimension contributes the diffusion.

Such the nonlinear diffusion due to crossing angle were not seen in the case of collision with zero crossing angle. There was no diffusion for not only Gaussian strong beam but also distorted beam as is shown in Figure 13. We remember that the diffusion at zero crossing angle was very weak for its pure Hamiltonian

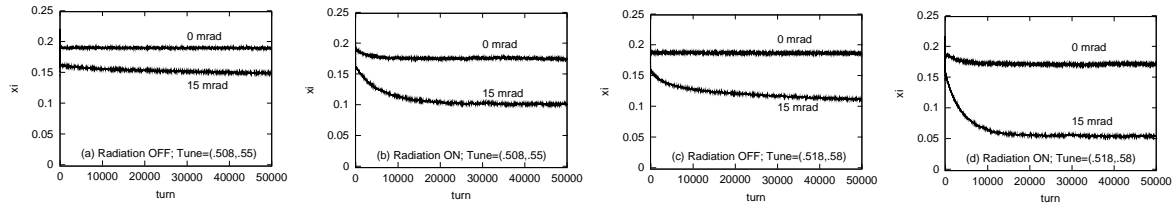


Figure 17: Diffusion due to crossing angle. Pictures (a) and (b) are depicted luminosity evolutions with/without synchrotron radiation damping, respectively, for tune operating point of (0.508,0.55). Pictures (c) and (d) are depicted with/without synchrotron radiation damping, respectively, for the tune operating point (0.518,0.58).

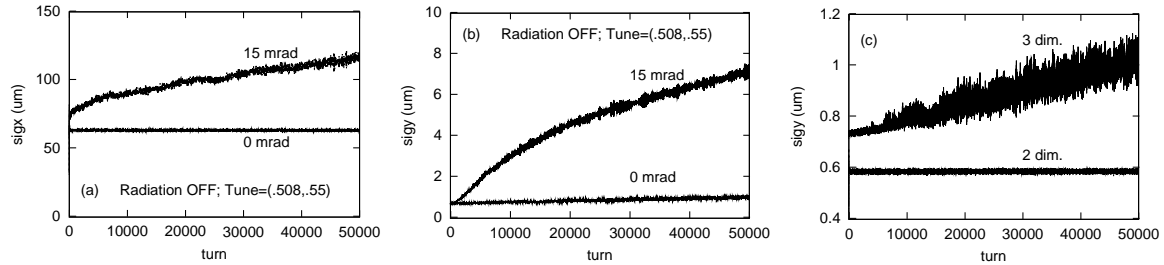


Figure 18: Diffusion of horizontal and vertical beam size due to crossing angle. Pictures (a) and (b) are depicted evolutions of horizontal and vertical beam sizes, respectively. Picture (c) is depicted diffusion seen in two and three dimensional simulations for zero-crossing angle and no synchrotron radiation.

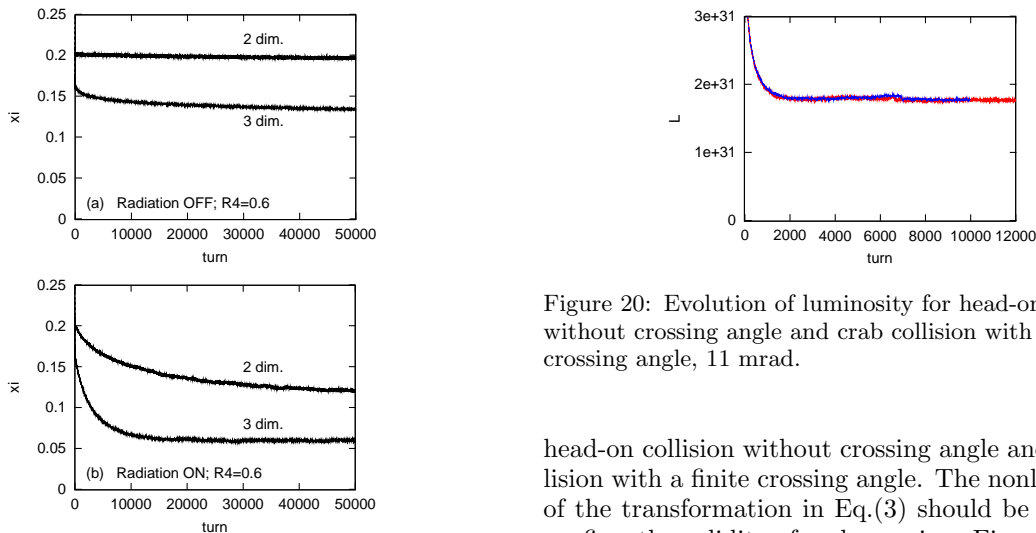


Figure 19: Diffusion of luminosity horizontal and vertical beam size due to crossing angle. Pictures (a) and (b) are depicted evolutions of the beam-beam parameter with and without synchrotron radiation, respectively. In each picture, two lines correspond to two and three dimensional simulations.

Figure 20: Evolution of luminosity for head-on collision without crossing angle and crab collision with a finite crossing angle, 11 mrad.

system but was enhanced by synchrotron radiation strongly. It should be note that the simulation was based on two dimensional PIC model. It is interesting to see the nonlinear diffusion for three dimensional PIC model.

So far, we neglected the difference between true

head-on collision without crossing angle and crab collision with a finite crossing angle. The nonlinear term of the transformation in Eq.(3) should be studied to confirm the validity of crab crossing. Figure 20 shows the luminosity evolution for head-on collision without crossing angle and crab collision with a finite crossing angle, 11 mrad. Two lines completely agreed each other: that is, the crab collision realizes the same performance as head-on collision without crossing angle.

5. Beam-beam tail

We have to discuss beam-beam tail which affects beam life time [10, 11]. Weak-strong simulation is used for the estimation of the halo. The weak-strong simulation was done with 500 macro-particle and 10^6

turns. Figure 21 shows particle distribution of beam

As is discussed in previous section, a deviation from Gaussian distribution was essential in the beam-beam limit for the luminosity. The mechanism of the luminosity limit was due to diffusion of particle distribution. The same mechanism should affect halo formation, namely the beam life time. PIC simulation is also essential for the halo prediction.

6. Summary

Mechanisms of the beam-beam limit has been discussed using various simulation methods. Coherent motion can be one of origins of the beam-beam limit. In our simulation, coherent motion limited the luminosity for short bunch length $\sigma_z < \beta_y/2$. The coherent motion disappear for longer bunch length perhaps due to the tune spread along the bunch length.

When the coherent motion is smeared, coherent effect limited the luminosity. Particle distribution of colliding beams is distorted by the beam-beam interaction, therefore the distortion limited the luminosity. We investigated pure nonlinear diffusion irrelevant to the radiation damping and excitation. For the collision without crossing angle, the diffusion is very weak not only for Gaussian beam but also for distorted beam. Radiation excitation enhances beam size enlargement for the distorted beam.

Crossing angle, x-y coupling or maybe other errors in the lattice of arc cause nonlinear diffusion due to coupling to the beam-beam interaction. The diffusion

was investigated for Gaussian beam. Perhaps it will be also seen for distorted beam. These studies are useful for the beam-beam limit in proton beam.

Acknowledgments

The authors wish to thank members of the super KEKB design working group for many fruitful discussions with them.

References

- [1] K. Yokoya and H. Koiso, Particle Accelerators, **27**, 181 (1990).
- [2] Y. Alexahin, FERMILAB-Conf-03/199 (2003).
- [3] K. Ohmi, Phys. Rev. **E62**, 7287 (2000).
- [4] M. Tawada, Y. Cai, K. Ohmi and J. Qiang, KEK-Preprint 2003-82 (2003).
- [5] J. Qiang, private communications (2003).
- [6] M. Bassetti and G. Erskine, CERN-ISR TH/80-06 (1980).
- [7] K. Ohmi, Proceedings of PAC03 (2003). (KEK-preprint 2003-95)
- [8] K. Oide and K. Yokoya, Phys. Rev. **A40**, 315 (1989).
- [9] K. Hirata, Phys. Rev. Letters, **74**, 2228 (1995).
- [10] T. Chen, J. Irwin and R. Siemann, Phys. Rev. **E49**, 2323 (1994).
- [11] D. Shatilov, Part. Accel., **52**, 65 (1996).

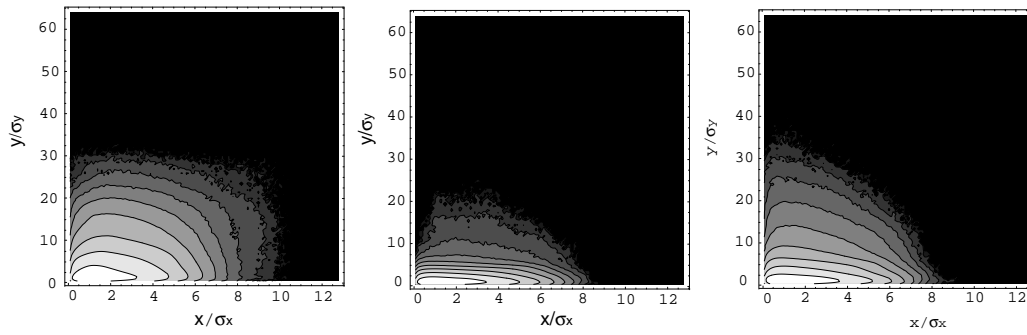


Figure 21: Contour plot of transverse particle density in a bunch obtained by the weak-strong simulation. Left and middle pictures are depicted for present KEKB parameter with and without crossing angle. Right picture is depicted for Super KEKB without crossing angle.